Anisotropic diffusion-based defect detection for low-contrast glass substrates

by

Du-Ming Tsai and Shin-Min Chao
Department of Industrial Engineering and Management
Yuan-Ze University, Taiwan, R.O.C.

Correspondence:

Du-Ming Tsai
Department of Industrial Engineering & Management
Yuan-Ze University
135 Yuan-Tung Road
Nei-Li, Tao-Yuan
Taiwan, R.O.C.

Fax: (03) 463-8907
E-mail: iedmtsai@saturn.yzu.edu.tw

Anisotropic diffusion-based defect detection for low-contrast glass substrates

Abstract

In this paper, we propose an anisotropic diffusion scheme to detect defects in low-contrast surface images and, especially, aim at glass substrates used in TFT-LCDs (Thin Film Transistor-Liquid Crystal Displays). In a sensed image of glass substrate, the gray levels of defects and background are hardly distinguishable and result in a low-contrast image. Therefore, thresholding and edge detection techniques cannot be applied to detect subtle defects in the glass substrates surface. Although the traditional diffusion model can effectively smooth noise and irregularity of a faultless background in an image, it can only passively stop the diffusion process to preserve the original low-contrast gray values of defect edges. The proposed diffusion method in this paper can simultaneously carry out the smoothing and sharpening operations so that a simple thresholding can be used to segment the intensified defects in the resulting image. The method adaptively triggers the smoothing process in faultless areas to make the background uniform, and performs the sharpening process in defective areas to enhance anomalies. Experimental results from a number of glass substrate samples including backlight panels and LCD glass substrates have shown the efficacy of the proposed diffusion scheme in low-contrast surface inspection.

Key words: Defect detection, Surface inspection, Anisotropic diffusion, Low-contrast images, Glass substrates

1. Introduction

Surface inspection is an important part of quality control in manufacturing. The manual activity of inspection can be subjective and highly dependent on the experiences of human inspectors. In recent years, image analysis techniques have been increasingly used in industry for surface defect inspection, in which one has to detect small defects that appear as local anomalies in material surfaces. In this paper, we consider the task of automated visual inspection in low-contrast surfaces, and especially focus on the glass substrates used for Thin Film Transistor-Liquid Crystal Displays (TFT-LCDs). The inspection of defects in such panel surfaces ensures the display quality and improves the yield in LCD manufacturing. In the sensed image of a glass substrate, the gray levels of defects and background are hardly distinguishable and result in a low-contrast image. Therefore, simple surface inspection methods such as thresholding and edge detection are difficult to detect subtle defects in low-contrast glass substrate images.

Many defect detection systems aim at uniform surface images such as glass panels [1], sheet steel [2], aluminum strips [3] and web materials [4] using simple thresholding or edge detection techniques. Defects in these uniform images can be easily detected because commonly used measures usually have very distinct values. The surfaces of glass substrates are also a class of uniform images, but with low-contrast intensities. The main low-contrast glass substrates studied in this paper include backlight panels and LCD glass substrates. Figure 1 presents two types of such glass substrates used for LCD modules. Figure 1(a1) shows a faultless backlight panel surface, and Figure 1(b1) shows a defective version of the panel.

Figures 1(c1) and (d1), respectively, present a faultless and a defective LCD panel surfaces. It can be seen from Figures 1(b1) and (d1) that the defects are difficult to be found in the uniform background with low-contrast intensities. In order to visualize the subtle defects, gray values of glass substrate images are stretched between 0 and 255 for an 8-bit display. Figures 1(a2)-(d2) show the contrast-stretched images of Figures 1(a1)-(d1), respectively. The stretched glass-substrate images of Figures 1(b2) and (d2) show the defects clearly, but they also present the background texture and non-uniform illumination. Hence, to detect defects in such stretched images, we may need complicated texture analysis techniques rather than the simple thresholding method. Figures 1(a3)-(d3) illustrate the gradient images of Figures 1(a1)-(d1), respectively. These resulting images reveal that the characteristic of a low-contrast surface image invalidates the use of gradient magnitude to identify local anomalies.

In low-contrast surface images, a local defect has a smooth change of brightness from its neighboring region and, therefore, provides no clear edges to apply the gradient-based methods for defect detection. The non-uniform intensity of a faultless region and the low-contrast intensity of a defective region also deter the use of simple thresholding methods. It is extremely difficult to reliably identify small defects in low-contrast surface images without false detection of noise. Little research has been done on defect detection in low-contrast images. Ngan *et al.* [5] developed an automated vision system for patterned fabrics and repetitive patterned textures. Their system combined wavelet transform and golden image subtraction to detect small-size and low-contrast defects. The method requires a golden image for reference, so the detection performance is affected by environmental changes. Lee and Yoo [6] presented a complicated data fitting approach for detecting regional

defects of brightness unevenness in LCD panel surfaces. They first estimated the background surface of an inspection image using a low-order polynomial data fitting. Subtraction of the estimated background surface from the original image was then applied to find the threshold for binary segmentation. The resulting image was then post-processed by median filtering, morphological closing and opening to remove noise and refine the segmentation. The proposed method worked successfully to detect regional defects in low-contrast, non-textured TFT-LCD surface images. However, it is very computationally intensive because the background surface must be estimated recursively by eliminating one pixel at a time throughout the entire inspection image.

In this paper, we propose an anisotropic diffusion scheme to tackle the problem of defect inspection in low-contrast glass substrate images. Anisotropic diffusion was first proposed by Perona and Malik [7] for scale-space description of images and edge detection. It has been widely used as an adaptive edge-preserving smoothing technique for edge detection [8, 9], image restoration [10, 11], image smoothing [12, 13], image segmentation [14, 15] and texture segmentation [16].

The anisotropic diffusion approach is basically a modification of the linear diffusion (or heat equation), and the continuous anisotropic diffusion is given by

$$\frac{\partial \boldsymbol{I}_t(x,y)}{\partial t} = \mathrm{div}\left[\boldsymbol{c}_t(x,y)\cdot\nabla \boldsymbol{I}_t(x,y)\right] \qquad (1)$$

where $\boldsymbol{I}_t(x,y)$ refers to the image at time t, div the divergence operator, $\nabla \boldsymbol{I}_t(x,y)$ the gradient of the image, and $\boldsymbol{c}_t(x,y)$ the diffusion coefficient. If $\boldsymbol{c}_t(x,y)$ is a

constant, equation (1) is reduced to the isotropic diffusion equation. It is then equivalent to convolving with a Gaussian function. The idea of anisotropic diffusion is to adaptively choose $\boldsymbol{c}_t$ such that intra-regions become smooth while edges of inter-regions are preserved. The diffusion coefficient $\boldsymbol{c}_t$ is generally selected to be a nonnegative function of gradient magnitude so that small variations in intensity such as noise or shading can be well smoothed, and edges with large intensity transition are retained.

You *et al*. [17] gave an in-depth analysis of the behavior of the Perona-Malik anisotropic diffusion model (P-M model) by considering the anisotropic diffusion as the steepest descent method for solving an energy minimization problem. Barash [18] addressed the fundamental relationship between anisotropic diffusion and adaptive smoothing. He showed that an iteration of adaptive smoothing

$$\boldsymbol{I}_{t+1}(x,y) = \frac{\sum_i \sum_j \boldsymbol{I}_t(x+i,y+j) w_t(x+i,y+j)}{\sum_i \sum_j w_t(x+i,y+j)} \tag{2}$$

is an implementation of the discrete version of the anisotropic diffusion equation if the weight w_t in eq. (2) is taken as the same of the diffusion coefficient $\boldsymbol{c}_t$ in eq. (1). Gilboa *et al*. [19] proposed a forward and backward (FAB) adaptive diffusion process to enhance edge and smooth noise in the image. The FAB diffusion model involves four *ad hoc* parameters, of which two critical threshold values of gradient must be manually and carefully chosen for the success of the diffusion result. The smaller threshold value determines the use of a forward function, while the larger threshold value determines the use of a backward function. A discontinuous

diffusion function is, therefore, applied since nothing is done for the gradient magnitude between the two threshold values.

The conventional diffusion model can effectively perform adaptive smoothing for intra-regions in an image. However, it can only passively stop the diffusion process to preserve original gray values of edges in inter-regions. For defect detection in a low-contrast image, the conventional diffusion model can only smooth the faultless background, but can not enhance the low-contrast defects. The diffused result may still be a low-contrast image. In this paper, we propose an improved anisotropic diffusion model that aims to enhance the gray-level difference between local anomalies and the background to detect defects in low-contrast glass substrate images. The proposed method automatically activates a smoothing process in faultless regions to make the background uniform, and performs a sharpening process in defective regions to enhance anomalies. The proposed method presents a unified continuous diffusion coefficient function that can adaptively carry out smoothing or sharpening operation with only two parameters for defect detection in low-contrast Images. It can distinctly enhance low-contrast defects and uniformly smooth the background without intensifying textured patterns and uneven illumination so that a simple binary thresholding can be effectively and efficiently applied to segment defects in the diffused image.

This paper is organized as follows. In section 2, we first review the Perona-Malik anisotropic diffusion equation, and then discuss the improved diffusion model that adaptively performs the smoothing and sharpening operations. Section 3 presents the experimental results from a variety of backlight panel and LCD glass substrate surfaces that contain various defects. The effect of varying diffusion

parameter values is also analyzed. Finally, section 4 gives a brief conclusion of our research.

2. The improved anisotropic diffusion model

2.1 Perona-Malik anisotropic diffusion model

Let $\boldsymbol{I}_t(x,y)$ be the gray level at coordinates (x,y) of a digital image at iteration t, and $\boldsymbol{I}_0(x,y)$ the original input image. The continuous anisotropic diffusion in eq. (1) can be discretely implemented by using four nearest neighbors and the Laplacian operator [7]:

$$\boldsymbol{I}_{t+1}(x,y) = \boldsymbol{I}_t(x,y) + \frac{1}{4}\sum_{i=1}^{4}[\boldsymbol{c}_t^i(x,y)\cdot\nabla\boldsymbol{I}_t^i(x,y)] \tag{3}$$

where $\nabla\boldsymbol{I}_t^i(x,y)$, i = 1, 2, 3 and 4, represent the gradients of four neighbors in the north, south, east and west directions, respectively, i.e.,

$$\nabla\boldsymbol{I}_t^1(x,y) = \boldsymbol{I}_t(x,y-1) - \boldsymbol{I}_t(x,y)$$

$$\nabla\boldsymbol{I}_t^2(x,y) = \boldsymbol{I}_t(x,y+1) - \boldsymbol{I}_t(x,y)$$

$$\nabla\boldsymbol{I}_t^3(x,y) = \boldsymbol{I}_t(x+1,y) - \boldsymbol{I}_t(x,y)$$

$$\nabla\boldsymbol{I}_t^4(x,y) = \boldsymbol{I}_t(x-1,y) - \boldsymbol{I}_t(x,y)$$

and $\boldsymbol{c}_t^i(x,y)$ is the diffusion coefficient associated with $\nabla\boldsymbol{I}_t^i(x,y)$. In the P-M

model, $\boldsymbol{c}_{\mathrm{t}}^{\mathrm{i}}(x,y)$ is considered as a function of the gradient $\nabla \boldsymbol{I}_{\boldsymbol{t}}^{i}(x,y)$, i.e.,

$$\boldsymbol{c}_{\mathrm{t}}^{\mathrm{i}}(x,y) = g(\nabla \boldsymbol{I}_{\mathrm{t}}^{\mathrm{i}}(x,y))$$

For the sake of simplicity, $\nabla \boldsymbol{I}_{\boldsymbol{t}}^{i}(x,y)$ is subsequently denoted by $\nabla \boldsymbol{I}$. The function $g(\nabla \boldsymbol{I})$ has to be a nonnegative, monotonically decreasing function with $g(0)=1$ and $\lim_{|\nabla I|\to\infty} g(\nabla \boldsymbol{I}) = 0$. The function $g(\nabla \boldsymbol{I})$ should result in low coefficient values at high-gradient edges to preserve the gray levels of edges, and high coefficient values for low-gradient pixels within an image region so that the region can be smoothed. In the P-M anisotropic diffusion model, a possible diffusion coefficient function is given by

$$g(\nabla \boldsymbol{I}) = 1/[1 + (|\nabla \boldsymbol{I}|/\mathcal{K})^2] \tag{4}$$

where the parameter $\mathcal{K}$ is a constant, and acts as an edge strength threshold.

Parameter $\mathcal{K}$ in the diffusion coefficient function must be fine-tuned for a particular application. If the $\mathcal{K}$ value is too large, the diffusion process will oversmooth and result in a blurred image. In contrast, if the $\mathcal{K}$ value is too small, the diffusion process will stop smoothing in early iterations and yield a restored image similar to the original one.

Let $\phi(\nabla \boldsymbol{I})$ be a flux function [7] defined as

$$\phi(\nabla \boldsymbol{I}) = g(\nabla \boldsymbol{I}) \cdot \nabla \boldsymbol{I} \tag{5}$$

A large flux value indicates a strong effect of smoothness. Figures 2 and 3 depict the diffusion coefficient function and the flux function in eqs. (4) and (5), respectively. For a given $\mathcal{K}$ value, it can be seen from Figure 2 that the diffusion coefficient function in eq. (4) drops dramatically and approximates to zero when the gradient magnitude $|\nabla \boldsymbol{I}|$ is larger than $4\mathcal{K}$. That is, the diffusion stops as soon as $|\nabla \mathrm{I}| > 4\mathcal{K}$. The maximum smoothness occurs at $|\nabla \boldsymbol{I}| = 1\mathcal{K}$, as shown in the corresponding flux function in Figure 3. The classical P-M model can effectively smooth intra-regions in an image. However, it can only stop the diffusion process to preserve the original gray values of edges in inter-regions. In a low-contrast image, the P-M model can smooth the faultless background but can not distinctly enhance subtle defects. Therefore, the diffusion result may still be a low-contrast image and defects cannot be reliably identified in the diffused image. Figures 4(a1) and (b1) present a faultless and a defective backlight panels, and Figures 4(a2) and (b2) are the respective contrast-stretched images. Figures 4(a3) and (b3) show the restoration results after 30 iterations of the diffusing process using the P-M model with a properly selected parameter value $\mathcal{K} = 1$. It can be found from the figure that the faultless area is uniform, but the defects remain invisible in the diffused image. This indicates that the traditional P-M model can not sufficiently enhance hardly-visible anomalies by simply smoothing low-gradient regions and passively preserving high-gradient edges. It is not an acceptable result for low-contrast glass substrate inspection.

2.2 The proposed anisotropic diffusion model

In this study, the objective is to detect subtle defects in low-contrast surface images. Observing the backlight panel images in Figures 1(b1) and 4(b1), we found the gray levels of defects and the faultless background are hardly distinguishable. In order to enhance the subtle defects effectively in a low-contrast image, we incorporate the sharpening process in the classical diffusion model. The proposed diffusion model not only provides different degrees of smoothing for intra-regions but also actively provides different degrees of sharpening for edges in inter-regions. The new diffusion model proposed in this study is given by

$$\begin{aligned} \boldsymbol{I}_{t+1}(x,y) = \boldsymbol{I}_{t}(x,y) &+ \frac{1}{4}\sum_{i=1}^{4}[g(\nabla \boldsymbol{I}_t^i(x,y))\cdot \nabla \boldsymbol{I}_t^i(x,y)] \\ &- \frac{1}{4}\sum_{i=1}^{4}[v(\nabla \boldsymbol{I}_t^i(x,y))\cdot \nabla \boldsymbol{I}_t^i(x,y)] \end{aligned} \tag{6}$$

The proposed diffusion model in eq. (6) unifies both the smoothing and sharpening processes in one single equation. The diffusion and sharpening strengths are adaptively adjusted by the diffusion coefficient function g and the sharpening coefficient function v. The second term on the right hand side of eq. (6) is the same classical diffusion process as the P-M model in eq. (3), and the third term is interpreted as the sharpening operation. In the proposed diffusion model of eq. (6), the sharpening coefficient function $v(\nabla \boldsymbol{I})$ has to be a nonnegative monotonically increasing function with $v(0)=0$ and $\lim_{|\nabla I|\to\infty} v(\nabla \boldsymbol{I}) = 1$. This function $v(\nabla \boldsymbol{I})$ should result in high coefficient values at edges that have relatively high gradient magnitudes so that they can be distinctly enhanced. It must generate low coefficient values for pixels within image regions that have low gradient magnitudes to inhibit

the sharpening process. In this study, the sharpening coefficient function $v(\nabla \boldsymbol{I})$ is defined as

$$v(\nabla \boldsymbol{I}) = \alpha \cdot [1 - g(\nabla \boldsymbol{I})] \tag{7}$$

where α is the weight of sharpening coefficient function with $0 \le \alpha \le 1$. This weighting factor determines the degree of sharpening with respect to the diffusion coefficient. The diffusion coefficient function $g(\nabla \boldsymbol{I})$ is the same as that defined in eq. (4). Note that the value of $g(\nabla \boldsymbol{I})$ ranges between 0 and 1. Eq. (6) can be reformulated as

$$\boldsymbol{I}_{t+1}(x,y) = \boldsymbol{I}_t(x,y) + \frac{1}{4}\sum_{i=1}^{4}[g(\nabla \boldsymbol{I}_t^i) - v(\nabla \boldsymbol{I}_t^i)]\nabla \boldsymbol{I}_t^i \tag{8}$$

Then $g(\nabla \boldsymbol{I}) - v(\nabla \boldsymbol{I})$ is the new diffusion coefficient function in the proposed diffusion model. Figures 5 and 6, respectively, depict the diffusion coefficient function $g(\nabla \boldsymbol{I}) - v(\nabla \boldsymbol{I})$ and the flux function $\phi(\nabla \boldsymbol{I}) = [g(\nabla \boldsymbol{I}) - v(\nabla \boldsymbol{I})] \cdot \nabla \boldsymbol{I}$ for the proposed diffusion model. For given α and $\mathcal{K}$ values, it can be seen from Figure 5 that the diffusion coefficient function $g(\nabla \boldsymbol{I}) - v(\nabla \boldsymbol{I})$ drops dramatically and shows a zero-crossing when the gradient magnitude $|\nabla \boldsymbol{I}|$ is larger than $\mathcal{K}/\sqrt{\alpha}$. In the flux function of the P-M model as shown in Fig. 3, the flow increases with the gradient strength to a peak and then slowly decreases to zero. This behavior implies that the diffusion process of the P-M model performs heavy smoothing for lower gradient areas (such as the uniform background) and carries out light smoothing (or stops the smoothing) for higher gradient areas (such as defects). Since the diffusion coefficient can only have a minimum value approximate to zero, the P-M model can

only passively preserve the original gray-levels of edges. It cannot aggressively enhance the edges of a defect to intensify the gray-level difference from the smoothed background. In contrast, the flux function of the proposed diffusion model in Figure 6 shows that the flow increases with the gradient strength to reach a maximum. It then decreases and crosses zero to negative values. This behavior indicates that the diffusion process performs smoothing for lower gradient areas (when $|\nabla \boldsymbol{I}| < \mathcal{K}/\sqrt{\alpha}$) and proceeds sharpening for higher gradient area (when $|\nabla \boldsymbol{I}| > \mathcal{K}/\sqrt{\alpha}$). When the diffusion coefficient becomes negative, the proposed diffusion model then actively performs the sharpening process. For defect detection in a low-contrast image, the model can effectively enhance defects in the diffused image.

As demonstrated in Figures 5 and 6 with $\alpha = 0.1$, the plots indicate that the proposed diffusion model will provide the smoothing process when $|\nabla \boldsymbol{I}| < 3.16\mathcal{K}$, and carry out the sharpening process when $|\nabla \boldsymbol{I}| > 3.16\mathcal{K}$. From the corresponding flux function in Figure 6, it shows that the maximum smoothness is at $|\nabla \boldsymbol{I}| = 1\mathcal{K}$. The sharpness strength is proportional to the gradient magnitude when $|\nabla \boldsymbol{I}| > 3.16\mathcal{K}$. In a low-contrast backlight panel, the gradient of a faultless background area is slightly smaller than that of the defective area. Therefore, if we can select appropriate parameter values for α and $\mathcal{K}$, the gradient of a faultless background area will fall in region A (i.e., $|\nabla \boldsymbol{I}| < 3.16\mathcal{K}$) as marked in Figure 6. Then the proposed diffusion model will carry out the smoothing process to make the background area uniform. Conversely, the gradient of a defective area will be located in region B (i.e., $|\nabla \boldsymbol{I}| > 3.16\mathcal{K}$) as shown in Figure 6, and the diffusion model

will perform the sharpening process to enhance edges in the defective area. The proposed diffusion model can automatically and adaptively trigger the smoothing or sharpening process based on the variations of gradient in the image with properly selected parameter values α and $\mathcal{K}$. The resulting diffusion image of an inspection surface will have a uniform background for the faultless region and distinct gray levels for the defective region. A simple thresholding can thus be applied to segment defects in the diffused image.

In order to explain the difference between the proposed diffusion model and the traditional P-M model, assume that the values of $\nabla \boldsymbol{I}/\mathcal{K}$ in the faultless background and the defective area are 2 and 4, respectively. Note that when $\alpha = 0.1$, the zero-crossing point occurs at $|\nabla \boldsymbol{I}| = 3.16\mathcal{K}$ in Figure 6. Comparing the flux functions in Figure 3 (the P-M model) and Figure 6 (the proposed model), the P-M model will generate a flux value of 0.4 in the faultless background area, but it gives a flux value of 0.24 in the defective area. This indicates that the P-M model carries out the smoothing process in both the faultless background and defective area with different diffusion strengths. In this case, both the faultless background area and the subtle defect are filtered out by the traditional P-M model. Conversely, the proposed diffusion model will generate a flux value of 0.24 in the faultless background area and -0.14 in the defective area. The positive flux value causes a smoothing process in the faultless background area and the negative flux value results in a sharpening process in the defective area. It can simultaneously smooth the faultless background area and enhance the subtle defect in an inspection image.

Since the parameters α and $\mathcal{K}$ of the proposed diffusion model in eq. (6)

must be fine-tuned for different applications, the following experiments are performed to determine the suitable values of α and $\mathcal{K}$ for defect detection in low-contrast surface images. Figure 7 shows the diffusion results of the test image of the defective backlight panel in Figure 1(b1) under various combinations of α and $\mathcal{K}$ values. The number of iterations is set to 30 for the test image. When the weight α is too small (i.e., the sharpening process in eq. (6) is inhibited), the defective region cannot be enhanced in the resulting diffusion image, as seen in Figures 7(a)-(f) with $\alpha = 0$ or $\alpha = 0.1$. Note that the diffusion results of Figures 7(a)-(c) with α=0 are equivalent to those from the P-M model. In contrast, when α is too large, the diffusion result in Figure 7(j) with $\alpha = 0.3$ shows that the proposed diffusion model will over-sharpen the image. When the diffusion parameter $\mathcal{K}$ is overly large with respect to a given α value, the resulting images are severely smoothed. The background area of the test image in Figure 1 (b1) is smoothed, but the shape of the defect is also lost, as seen in Figures 7(c), (f), (i) and (l) with a large $\mathcal{K}$ value of 2. When the parameter $\mathcal{K}$ is overly small and α is too large, the results in Figures 7(g) and (j) show that the diffusion process generates many false sharpened objects and noise. Figure 7(h) shows a good diffusion result that enhances the hardly-visible defect and removes noise in the resulting image. Thus, $\alpha = 0.2$ and $\mathcal{K} = 1$ are suitable values to use for low-contrast backlight panel inspection. Since the surface structure of LCD glass substrates is different from backlight panels (see the contrast-stretched images in Figures 1(a2)-(d2)), we need another combination of α and $\mathcal{K}$ values for LCD glass substrate inspection. With the similar experiments, we found that the suitable combination for LCD glass substrate inspection is $\alpha = 0.2$ and $\mathcal{K} = 2$. As a general guideline, a larger $\mathcal{K}$ value is recommended for less-uniform or complicated surfaces. This is because that the faultless background area in those images usually has larger gradient magnitude. An α value of 0.2 has

generally performed well for enhancing local anomalies in a low-contrast image.

3. Experimental results

In this section, we present experimental results from a number of backlight panels and LCD glass substrates containing various low-contrast defects in images. The algorithm was implemented on a Pentium 4, 3G Hz personal computer using the Visual Basic language. The images were 200×200 pixels wide with 8-bit gray levels. The number of iterations was 30 for all test images in the experiments. Computation time of 30 iterations on a 200×200 image was 0.3 seconds.

Although a general guideline for the parameter settings of $\mathcal{K}$ and α has been given in section 2, we further provide practical selection rules of parameter values of $\mathcal{K}$ and α in the experiment. Given a low-contrast glass substrate image that contains anomalies, we can generally expect that the average gradient magnitude of the defective region is larger than that of a faultless region, and the overall mean gradient magnitude of the whole image is somewhere in between. If we set the parameter $\mathcal{K}$ to the mean gradient magnitude of the whole image, then the diffusion process will perform smoothing for faultless regions (lower gradient areas), and carry out sharpening for defective regions (higher gradient areas) simultaneously. Therefore, we can select the parameter $\mathcal{K}$ based on the mean gradient magnitude of the whole image. The mean gradient magnitude $\nabla\bar{\boldsymbol{I}}$ for an image of size $M\times N$ is defined as

$$\nabla\bar{\boldsymbol{I}}=\frac{1}{4MN}\sum_{x=0}^{M-1}\sum_{y=0}^{N-1}\sum_{i}^{4}\nabla\boldsymbol{I}^{i}(x,y) \tag{9}$$

In this paper, the parameter $\mathcal{K}$ is given by the nearest integer of $\nabla\bar{\boldsymbol{I}}$, i.e., $\mathcal{K} = \mathrm{Int}(\nabla\bar{\boldsymbol{I}} + 0.5)$. A thorough experiment from a variety of low-contrast glass substrate images has shown that the selected $\mathcal{K}$ works successfully for the defect detection application.

The parameter α is the sharpening weight factor with $0 \le \alpha \le 1$ in eq. (7). When α is set to zero, the proposed method is equivalent to the traditional P-M model that simply carries out adaptive smoothing. Merely smoothing faultless and noisy regions without sharpening defective areas cannot effectively enhance low-contrast anomalies on the inspection surface. Figure 8 shows the plots of four diffusion coefficient functions with $\alpha = 0.05, 0.1, 0.3$ and 0.5, in which the four corresponding zero-crossing points occur at $|\nabla \boldsymbol{I}| = 4.47\mathcal{K}, 3.16\mathcal{K}, 1.82\mathcal{K}$ and $1.41\mathcal{K}$, respectively. In low-contrast surface images, the average gradient magnitude of the defective region is between 2 and 3 times that of the whole image. If we set α to an excessively large value (e.g., α=0.5), then the proposed diffusion model will perform sharpening in early diffusion iterations and enhance both anomalies and details in the faultless area. In contrast, if α is set to an overly small value (e.g., α=0.05), then the proposed diffusion model carries out the sharpening operation too late and the defective area cannot be sufficiently enhanced. Therefore, it is suggested to use an α value between 0.1 and 0.3.

The selection guidelines of $\mathcal{K}$ and α have been applied to test samples of backlight panel surfaces, LCD glass substrates and LCD panel surface images, as shown in Figures 9, 10 and 11. The mean gradient magnitudes $\nabla\bar{\boldsymbol{I}}$ for the test images in Figures 9, 10 and 11 are ranged between 1.22~1.41, 1.52~1.91 and

0.69~0.75, respectively. The selected values of parameter $\mathcal{K}$ based on eq. (9) has been applied successfully for each test image in the experiment. The experimental results demonstrated that the selection rules of $\mathcal{K}$ and α can be applied successfully to all low-contrast surface images. The details of experimental results are discussed as follows.

The test images in Figures 9(a1)-(e1) present one faultless and four defective backlight panel images. The values of parameters α and $\mathcal{K}$ were set to fixed values of 0.2 and 1, respectively, based on the parameter selection rules above. Figures 9(a2)-(e2) present, respectively, the contrast-stretched images of Figures 9(a1)-(e1) so that the defect locations and shapes can be visibly observed. The results from the proposed diffusion model are shown in Figures 9(a3)-(e3). It can be seen that the shapes of defects are effectively highlighted in the diffused images. In order to segment defects in the diffused image, we use the simple statistical control limits to set up the thresholds. The upper and lower control limits for intensity variation in the diffused image are given by

$$\mu_d \pm S\sigma_d$$

where μ_d and σ_d are the mean and standard deviation of gray values in the whole diffused image, and S is a control constant. In the diffused image, if the gray level of a pixel falls within the control limits, the pixel is classified as a faultless point. Otherwise, it is classified as a defective one. In this study, the control constant $S=3$ is used for all test samples to follow the 3-sigma standard. Figures 9(a4)-(e4) illustrate the simple thresholding results of the diffused images in Figures 9(a3)-(e3) as binary images. The results reveal that the resulting image of the faultless

backlight panel surface is uniformly white, and the defects in all four defective surfaces are correctly segmented in the binarized images.

Figure 10 demonstrates further the detection results of LCD glass substrate images. The parameter values of α and $\mathcal{K}$ are respectively set to 0.2 and 2. Figure 10(a1) is a clear LCD image, and Figures 10(b1)-(e1) are four defective LCD images. It can be seen from the contrast-stretched images in Figures 10(a2)-(e2) that the LCD glass substrates contain a horizontal structural pattern with uneven lighting on the surfaces. The results from the proposed diffusion model are presented in Figures 10(a3)-(e3), which show that the irregular background is well smoothed and the defects are distinctly enhanced. Figures 10(a4)-(e4) show the thresholding results of the diffused images in Figures 10(a3)-(e3) using the 3-sigma control limits. The results also reveal that all local defects embedded in low-contrast surface images are effectively detected, and the resulting image of the clear surface image is uniformly white. The experiments have shown that the proposed diffusion scheme performs well in detecting subtle defects in low-contrast glass substrate images.

Figure 11 presents two additional LCD panel samples to demonstrate the effect of the two selected parameters $\mathcal{K}$ and α. Figures 11(a1) and (b1) show, respectively, a faultless image and a defective image with a blob-mura (brightness unevenness). Figures 11(a2) and (b2) illustrate the diffusion results with α=0.2 and $\mathcal{K}$=1. The thresholding results are presented in Figures 11(a3) and (b3). The detection results show that the selected values of $\mathcal{K}$ and α based on the previous selection guidelines are well suited for defect inspection of low-contrast surface images.

In order to demonstrate the superiority of using the proposed diffusion model for detecting defects in low-contrast glass substrate surfaces, Figures 12 and 13 compare the detection results of various filtering methods. Specifically, Laplacian sharpening filter, Sobel edge detection, bilateral filtering, the P-M diffusion model and the proposed diffusion model are used for comparison. Bilateral filtering [18, 20] is a newly developed edge-preserving smoothing technique that extends the concept of Gaussian smoothing by weighting the filter coefficients with their corresponding relative pixel intensities. Figures 12(a1) and 13(a1) are respectively the faultless and defective backlight panel surfaces used for evaluation. Figures 12(a2)-(a6) and 13(a2)-(a6) show the resulting diffusion images for Figures 12(a1) and 13(a1) from Laplacian, Sobel, bilateral filtering, P-M model and the proposed method, respectively. The corresponding thresholding results using 3-sigma control limits for the test images in Figures 12(a1)-(a6) and Figures 13(a1)-(a6) are illustrated in Figures 12(b1)-(b6) and 13(b1)-(b6). The resulting binary images in Figures 12(b2)-(b5) and 13(b2)-(b5) show that the Laplacian filtering, Sobel edge detection and bilateral filtering yield numerous noisy points in both faultless and defective test images, and the P-M model performs poorly because the anomalies in the defective images were severely smoothed. In contrast, as seen in Figures 12(b6) and 13(b6), the detection results from the proposed method show a uniformly white image for the faultless surface, while present the anomaly as an intensified region for the defective surface. Thus, the presenting diffusion process is essential for effective detection of small defects in low-contrast glass substrates.

To further demonstrate the usefulness of the proposed method, we also applied both the proposed diffusion model and the P-M diffusion model for defect detection in textured images. Figure 14 presents two additional textile fabric images, in which

Figure 14(a1) is a faultless fabric surface, and Figure 14(b1) is a defective one. The results from the traditional P-M diffusion model with varying values of $\mathcal{K}$ are shown in Figures 14(a2)-(a4) and 14(b2)-(b4). The resulting images of the proposed method with α=0.2 and $\mathcal{K}$=8 are presented in Figures 14(a5) and (b5). The number of iterations is set to 30 for both methods. In the P-M diffusion model, a small value of $\mathcal{K}$ (e.g., $\mathcal{K}$=2) provides only minor smoothing effect and, therefore, the detailed background texture still remains in the filter image, as seen in Figures 14(a2) and (b2). By setting the parameter $\mathcal{K}$ with a large value (e.g., $\mathcal{K}$=8), the P-M diffusion model oversmoothes both the texture background and local anomalies. The resulting defect region, as seen in Figures 14(a4) and (b4), are severely blurred. When a suitable $\mathcal{K}$ value (i.e., $\mathcal{K}$=4) is selected, the P-M diffusion model performs adaptive smoothing well. However, it can only filter out the structure texture, but cannot effectively enhance edges of the anomaly. This results in a blurred defect in the low-contrast uniform image, as seen in Figure 14(b3). Figures 14(a5) and (b5) show the results of the proposed method. They reveal that the proposed diffusion model not only smooth the texture surface as a uniform region but also distinctly enhance the local defect in the diffused images.

4. Conclusions

Detecting small defects which appear as local anomalies embedded in a homogeneous surface is a common problem in automated surface inspection in industry. The defects under inspection in this study are generally small in size and have no distinct intensity variations from their surrounding regions. Therefore, simple thresholding and gradient-based methods cannot be used to reliably identify such defects in low-contrast surface images. In this study, we have proposed an

improved version of anisotropic diffusion for detecting defects in glass substrate surfaces that involve low-contrast intensities in images.

Since the defects in low-contrast glass substrate surfaces are hardly visible, it makes the defect detection task extremely difficult. The traditional P-M diffusion model can effectively perform the smoothing process for the faultless background in an image. However, it can only passively stop the smoothing process to preserve original gray values of subtle defects. In order to enhance low-contrast defects, the sharpening process is incorporated in the proposed diffusion model. For given parameter values of α and $\mathcal{K}$, the proposed diffusion model can automatically and adaptively perform the smoothing or sharpening process in an image according to the local gradient magnitudes. It can effectively filter out the background noise in a faultless region, and yet well sharpen the anomalies in the diffused image. The diffused image of an inspection surface will have a uniform background for the faultless region and distinct gray levels for the defective region. A simple thresholding is thus easily applied to segment defects in the diffused image.

Experimental results from the backlight panels and LCD glass substrates have shown that the proposed anisotropic diffusion scheme can effectively detect small defects in low-contrast glass substrate surfaces. Although the proposed method in this paper mainly aims at defect detection in low-contrast surface images, it is believed that it can also be extended for image restoration in general. By choosing the suitable parameter values of α and $\mathcal{K}$, the proposed method can filter out noise and enhance the target object in the diffused image. In this study, the parameters of the proposed diffusion model must be fine-tuned for a specific application. The selection rules for parameter settings have been proposed in the experiment, and have worked

successfully for defect detection in various low-contrast surface images. Automatic parameter value setting based on the intensity characteristics and image content for more generic applications in image restoration is currently under investigation.

References

1. J. Wilder, Finding and evaluating defects in glass. In: Machine Vision for Inspection and Measurement, Ed. H. Freeman, Academic Press, New York, 1989, pp. 237-255.

2. J. Olsson, S. Gruber, Web process inspection using neural classification of scattering light, Proceedings of the IEEE International Conference on Industrial Electronics, Control, Instrumentation and Automation, San Diego, 1992, pp. 1443-1448.

3. C. Fernandez, C. Platero, P. Campoy, R. Aracil, Vision system for on-line surface inspection in aluminum casting process, Proceedings of the IEEE International Conference on Industrial Electronics, Control, Instrumentation and Automation, Maui, HA, 1993, pp. 1854-1859.

4. D. Brzakovic, N. Vujovic, Designing defect classification system: a case study, Pattern Recognition 29 (1996) 1401-1419.

5. Y.T. Ngan, G.K.H. Pang, S.P. Yung, K.P. Ng, Defect detection on patterned jacquard fabric, Proceedings of the 32nd Applied Imagery Pattern Recognition Workshop, Washington, DC, 2003, pp. 163-168.

6. J.Y. Lee, S.I. Yoo, Automatic detection of region-mura defect in TFT-LCD, IEICE Transactions on Information and Systems, E87-D (2004) 2371-2378.

7. P. Perona, J. Malik, Scale-space and edge detection using anisotropic diffusion, IEEE Transactions on Pattern Analysis and Machine Intelligence 12 (1990) 629-639.

8. L. Alvarez, P.L. Lions, J.M. Morel, Image selective smoothing and edge detection by nonlinear diffusion (II), SIAM Journal on Numerical Analysis 29 (1992) 845-866.

9. Y. Chen, C.A.Z. Barcelos, Smoothing and edge detection by time-varying coupled nonlinear diffusion equations, Computer Vision and Image Understanding 82 (2001) 85-100.

10. G. Sapiro, D.L. Ringach, Anisotropic diffusion of multivalued images with applications to color filtering, IEEE Transactions on Image Processing 5 (1996) 1582-1586.

11. A.F. Solé, A. López A, Crease enhancement diffusion, Computer Vision and

Image Understanding 84 (2001) 241-248.

12. F. Torkamani-Azar, K.E. Tait, Image recovery using the anisotropic diffusion equation, IEEE Transactions on Image Processing 5 (1996) 1573-1578.

13. H. Tsuji, T. Sakatani, Y. Yashima, N. Kobayashi, A nonlinear spatio-temporal diffusion and its application to prefiltering in MPEG-4 video coding, Proceedings of the International Conference on Image Processing I, 2002, pp. 85-88.

14. W.J. Niessen, K.L. Vincken, J.A. Weickert, M.A. Viergever, Nonlinear multiscale representations for image segmentation, Computer Vision and Image Understanding 66 (1997) 233-245.

15. S.A. Bakalexis, Y.S. Boutalis, B.G. Mertzios, Edge detection and image segmentation based on nonlinear anisotropic diffusion, IEEE International Conference on Digital Signal Processing 2, 2002, pp. 1203-1206.

16. H. Deng, J. Liu, Unsupervised segmentation of textured images using anisotropic diffusion with annealing function, International Symposium on Multimedia Information Processing, 2000, pp. 62-67.

17. Y.L. You, W. Xu, A. Tannenbaum, M. Kaveh, Behavioral analysis of anisotropic diffusion in image processing, IEEE Transactions on Image Processing 5 (1996) 1539-1553.

18. D. Barash, A fundamental relationship between bilateral filtering, adaptive smoothing, and the nonlinear diffusion equation, IEEE Transactions on Pattern Analysis and Machine Intelligence 24 (2002) 844-847.

19. G. Gilboa, N. Sochen, Y.Y. Zeevi, Forward-and-backward diffusion processes for adaptive image enhancement and denoising, IEEE Transactions on Image Processing 11 (2002) 689-703.

20. C. Tomasi, R. Manduchi, Bilateral filtering for gray and color images, IEEE International Conference on Computer Vision, Bombay, India, 1998, pp.839-846.

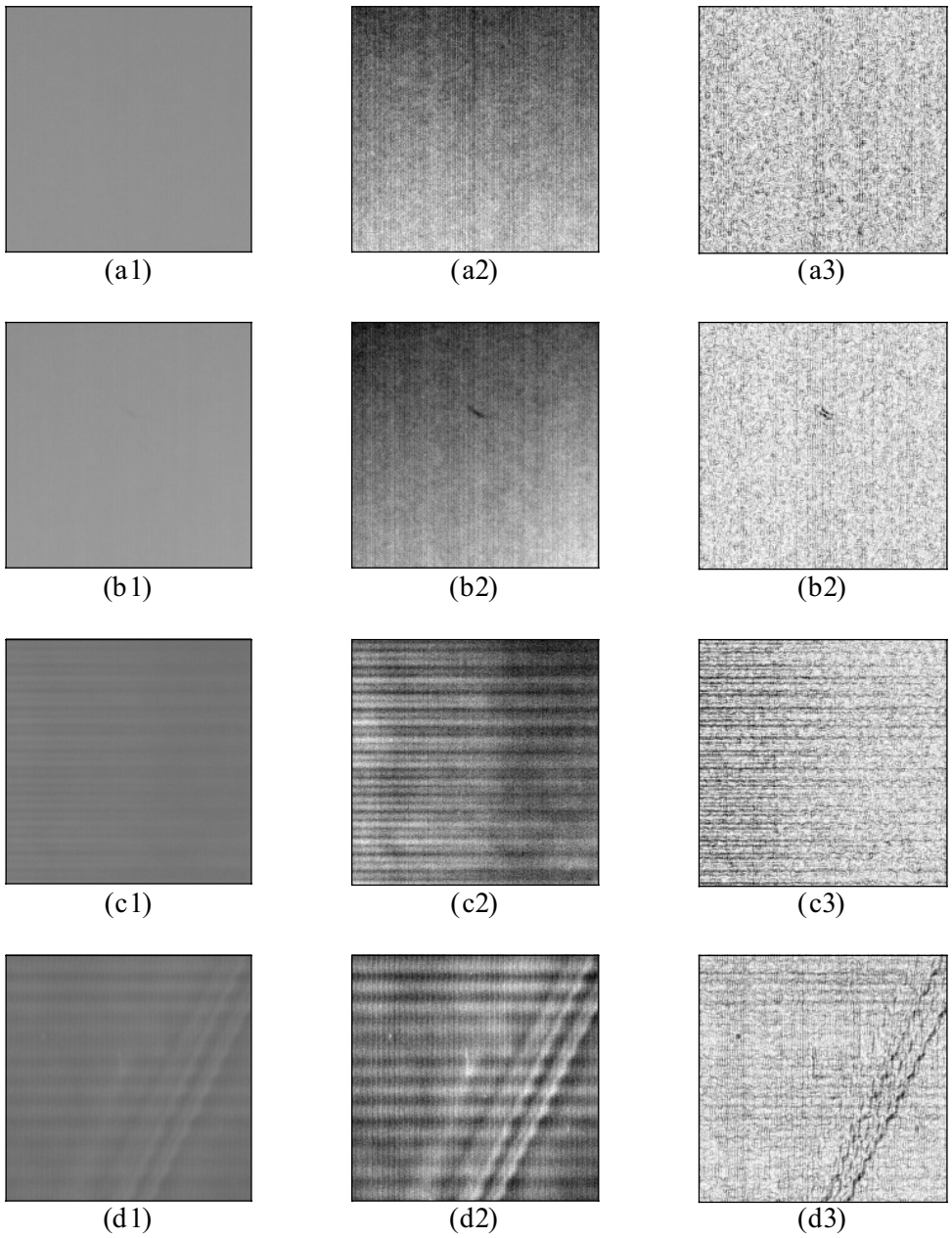

Figure 1. Surface images of glass substrates with low-contrast intensities: (a1), (b1) faultless and defective backlight panel images; (c1), (d1) faultless and defective LCD glass substrate images; (a2)-(d2) contrast-stretched images of (a1)-(d1), respectively; (a3)-(d3) respective gradient images of (a1)-(d1).

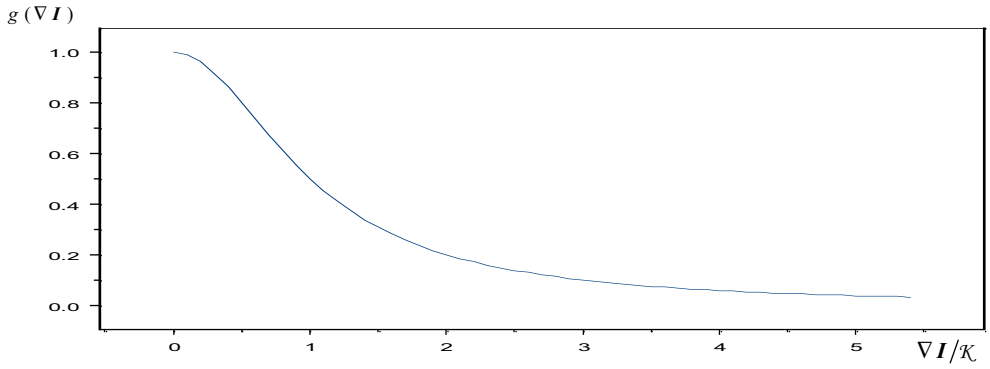

Figure 2. Graph of the diffusion coefficient function: $g(\nabla \boldsymbol{I}) = 1/[1+(|\nabla \boldsymbol{I}|/\mathcal{K})^2]$.

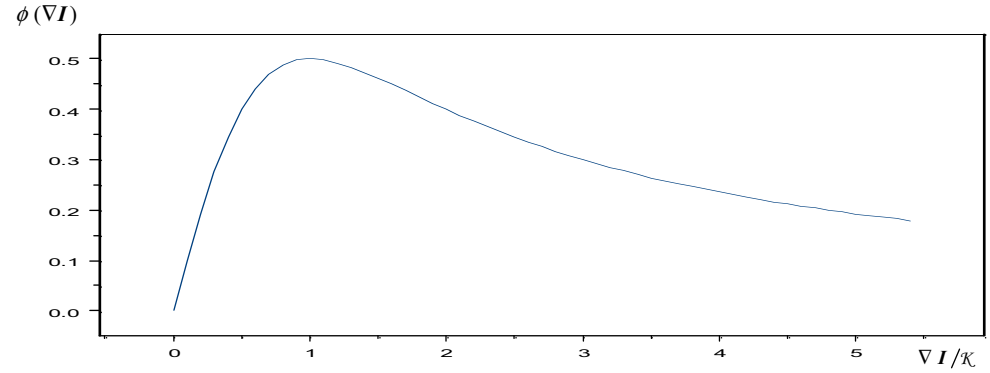

Figure 3. Graph of the flux function: $\phi(\nabla \boldsymbol{I}) = \{1/[1+(|\nabla \boldsymbol{I}|/\mathcal{K})^2]\} \cdot \nabla \boldsymbol{I}$.

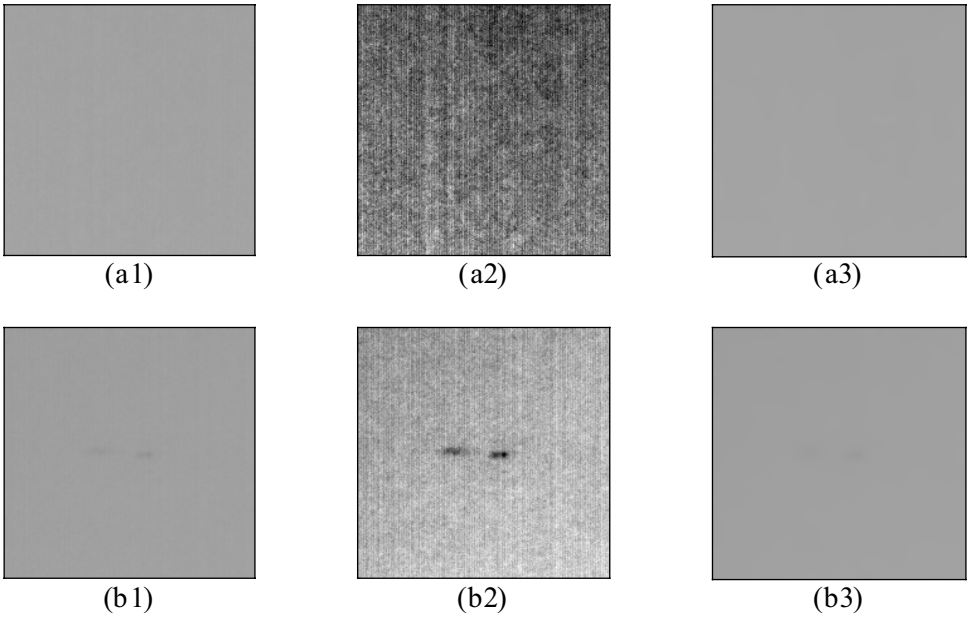

Figure 4. Diffusion results of the backlight panels using the P-M model: (a1) faultless image; (b1) defective image; (a2), (b2) contrast-stretched images of (a1) and (b1), respectively; (a3), (b3) respective diffused images of (a1) and (b1).

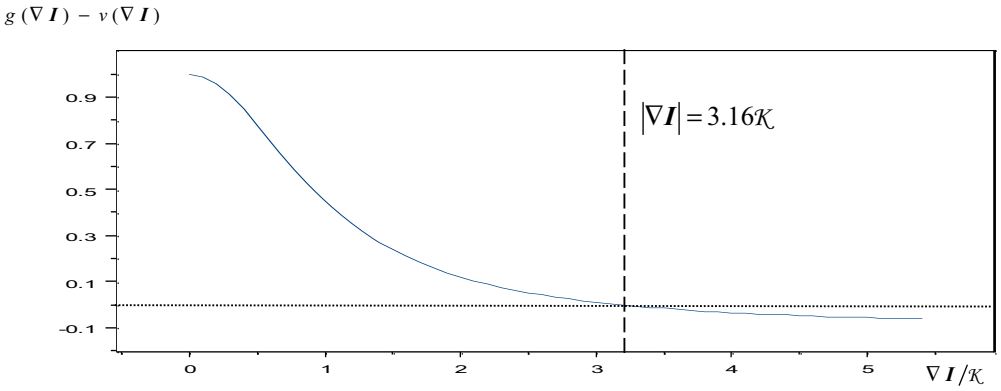

Figure 5. Graph of the diffusion coefficient function: $g(\nabla I) - v(\nabla I)$ with $\alpha = 0.1$.

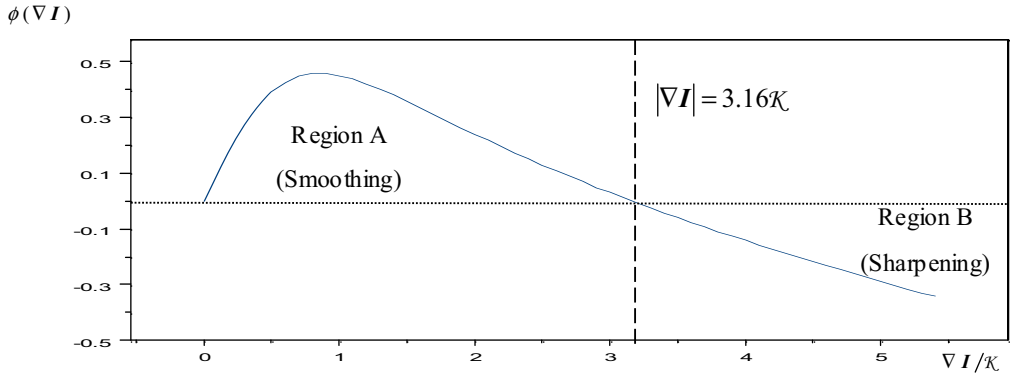

Figure 6. Graph of the flux function: $\phi(\nabla I) = [g(\nabla I) - v(\nabla I)] \cdot \nabla I$ with $\alpha = 0.1$.

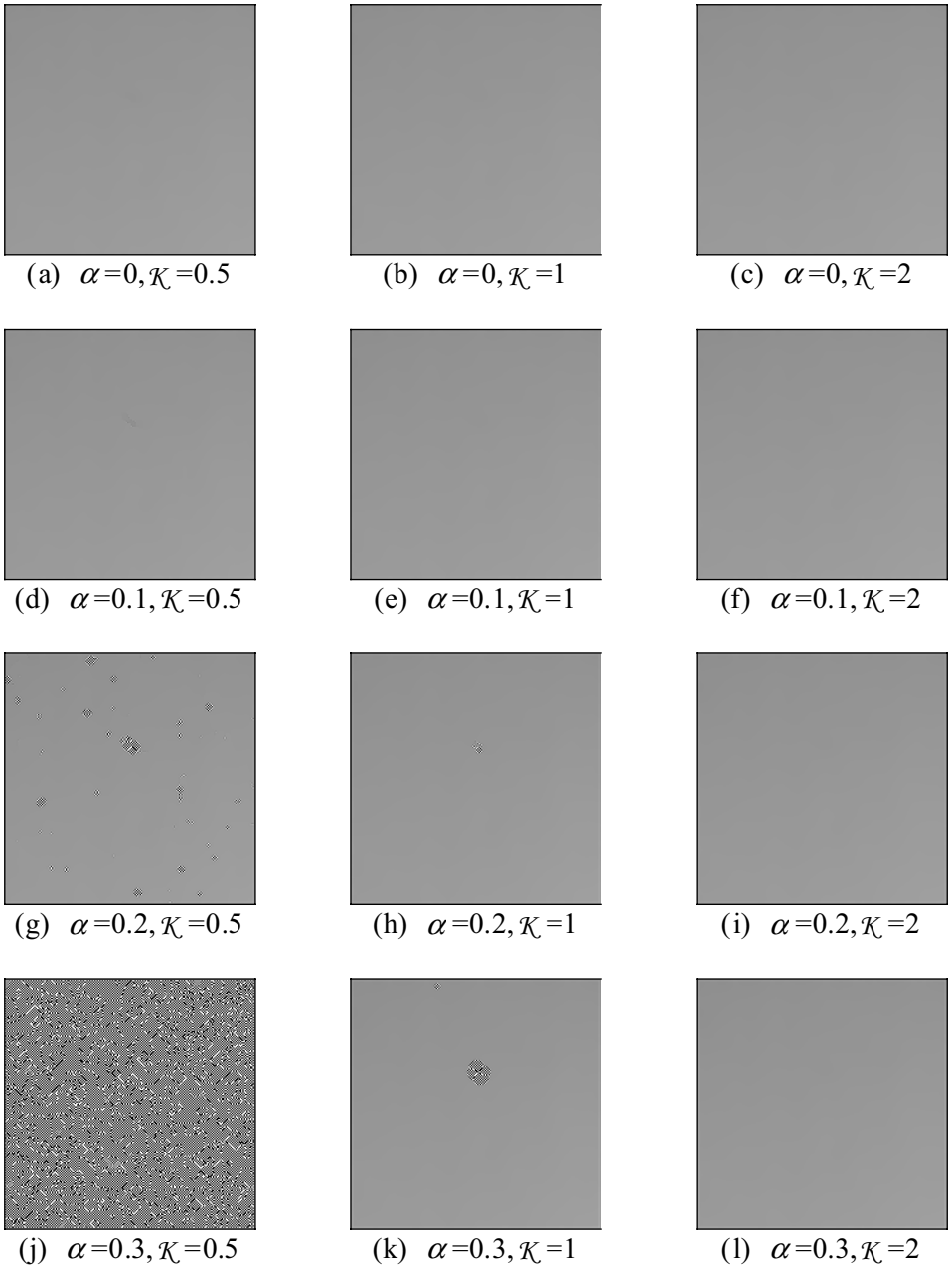

Figure 7. Diffusion results of the defective image in Figure 1(b1) under various combinations of α and $\mathcal{K}$. (The number of iterations is set to 30 for all tests.)

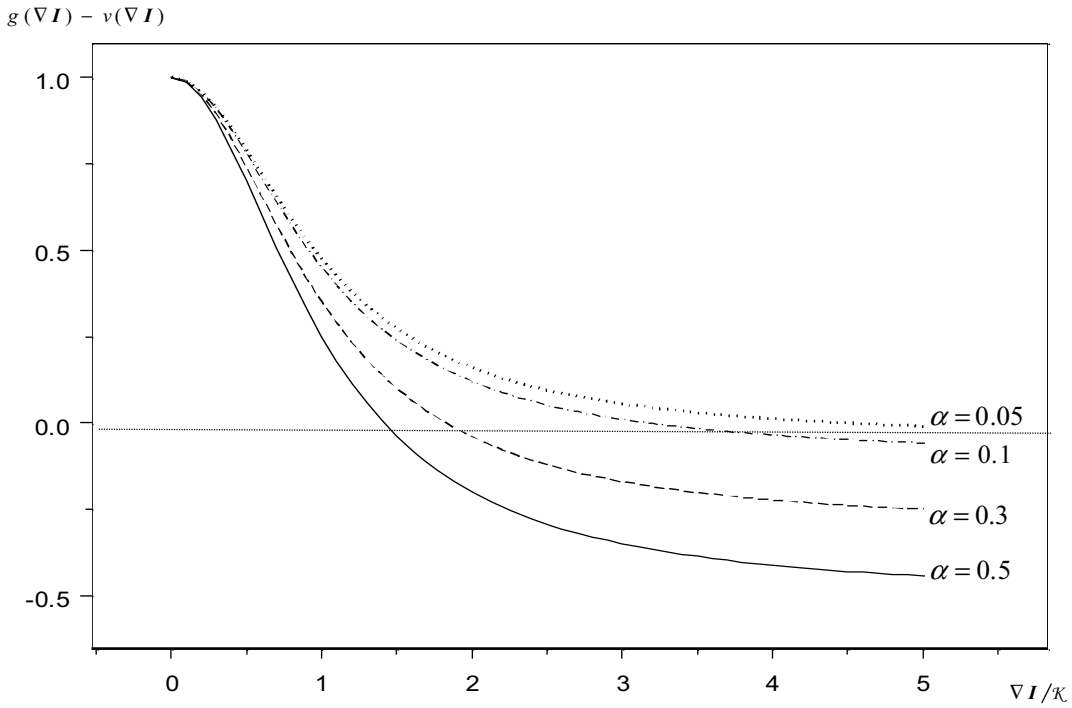

Figure 8. Plots of the diffusion coefficient function $g(\nabla \boldsymbol{I}) - v(\nabla \boldsymbol{I})$ with $\alpha = 0.05, 0.1, 0.3$ and 0.5.

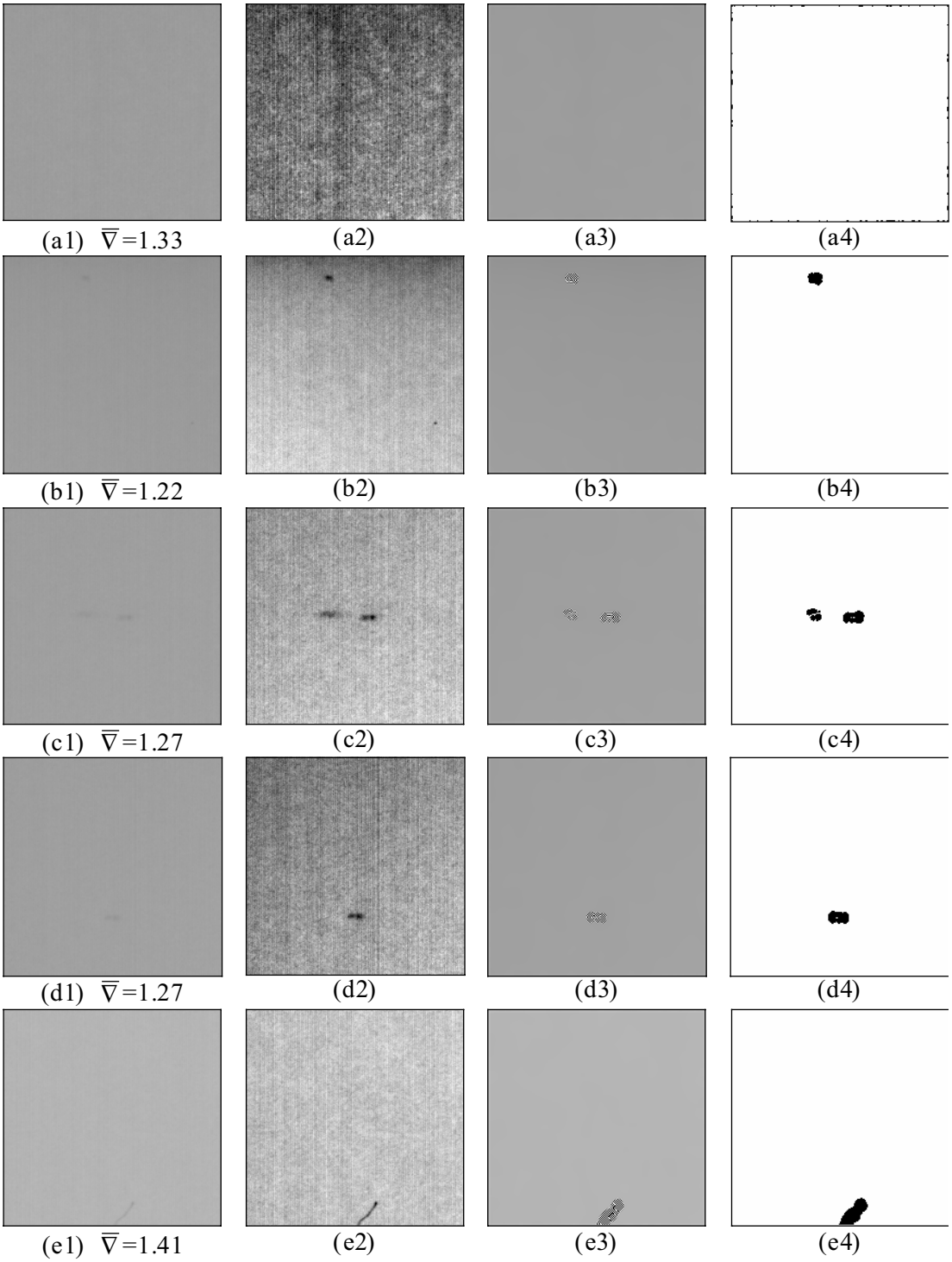

Figure 9. Diffusion results of backlight panel surfaces: (a1)-(e1) a faultless and four defective test images; (a2)-(e2) contrast-stretched images of (a1)-(e1), respectively; (a3)-(e3) respective diffusion results with α = 0.2 and $\mathcal{K}$ = 1 for all samples (number of iterations = 30); (a4)-(e4) thresholding results using 3-sigma control limits. ($\overline{\nabla}$ is the mean gradient magnitude defined in eq. (9).)

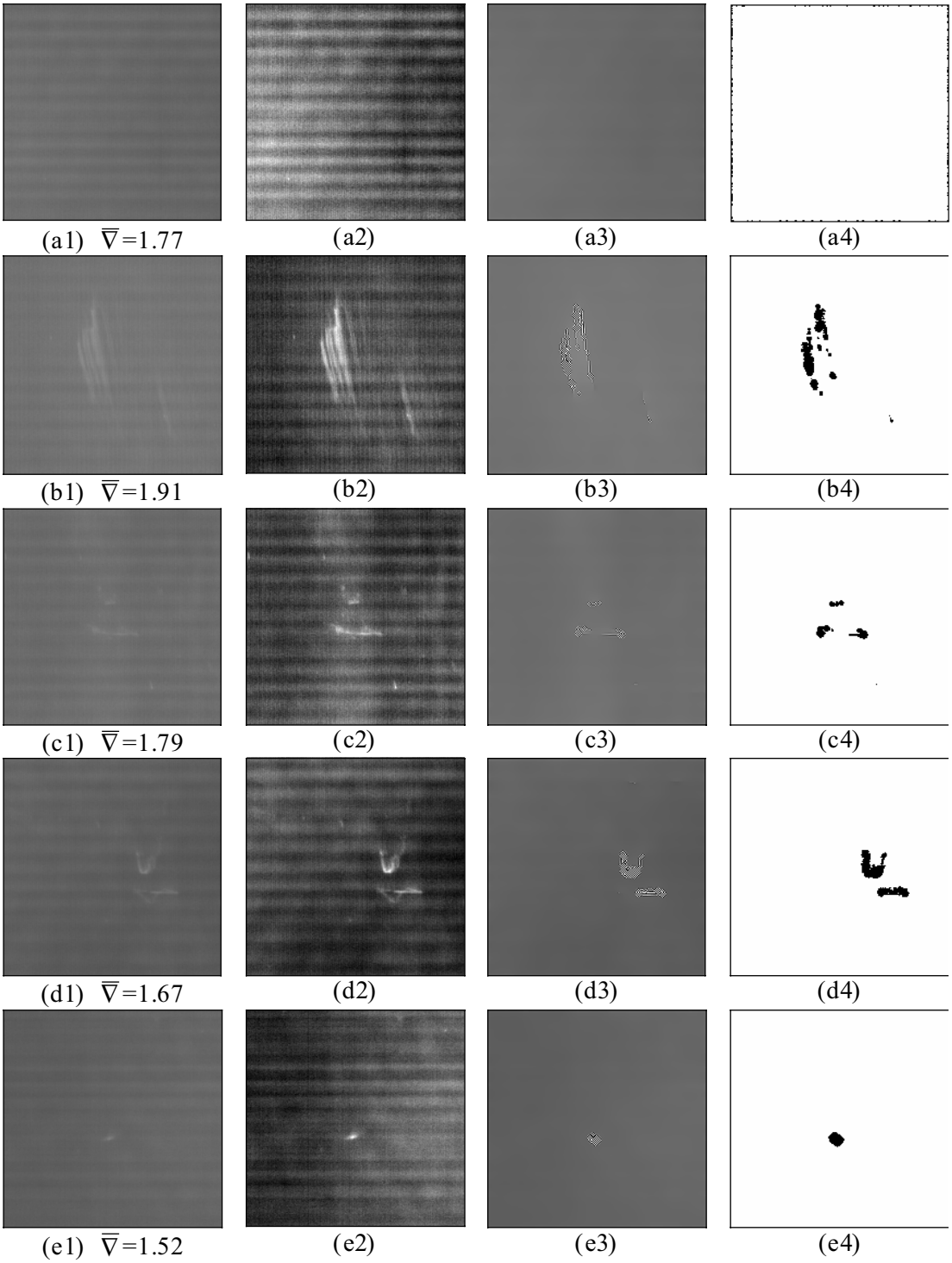

Figure 10. Diffusion results of LCD glass substrates: (a1)-(e1) a faultless and four defective test images; (a2)-(e2) contrast-stretched images of (a1)-(e1), respectively; (a3)-(e3) respective diffusion results with $\alpha = 0.2$ and $\mathcal{K} = 2$ for all samples (number of iterations = 30); (a4)-(e4) thresholding results using 3-sigma control limits.

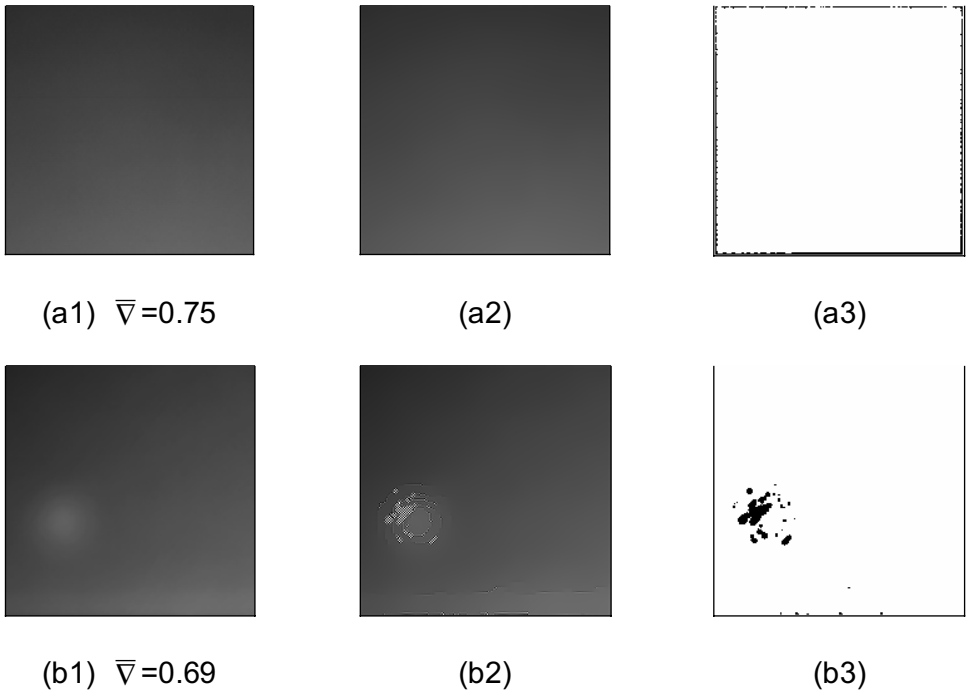

Figure 11. Diffusion results of mura samples: (a1)-(b1) faultless and defective test images; (a2)-(b2) respective diffusion results with α= 0.2 and $\mathcal{K}$= 1 (number of iterations = 30); (a3)-(b3) thresholding results using 3-sigma control limits.

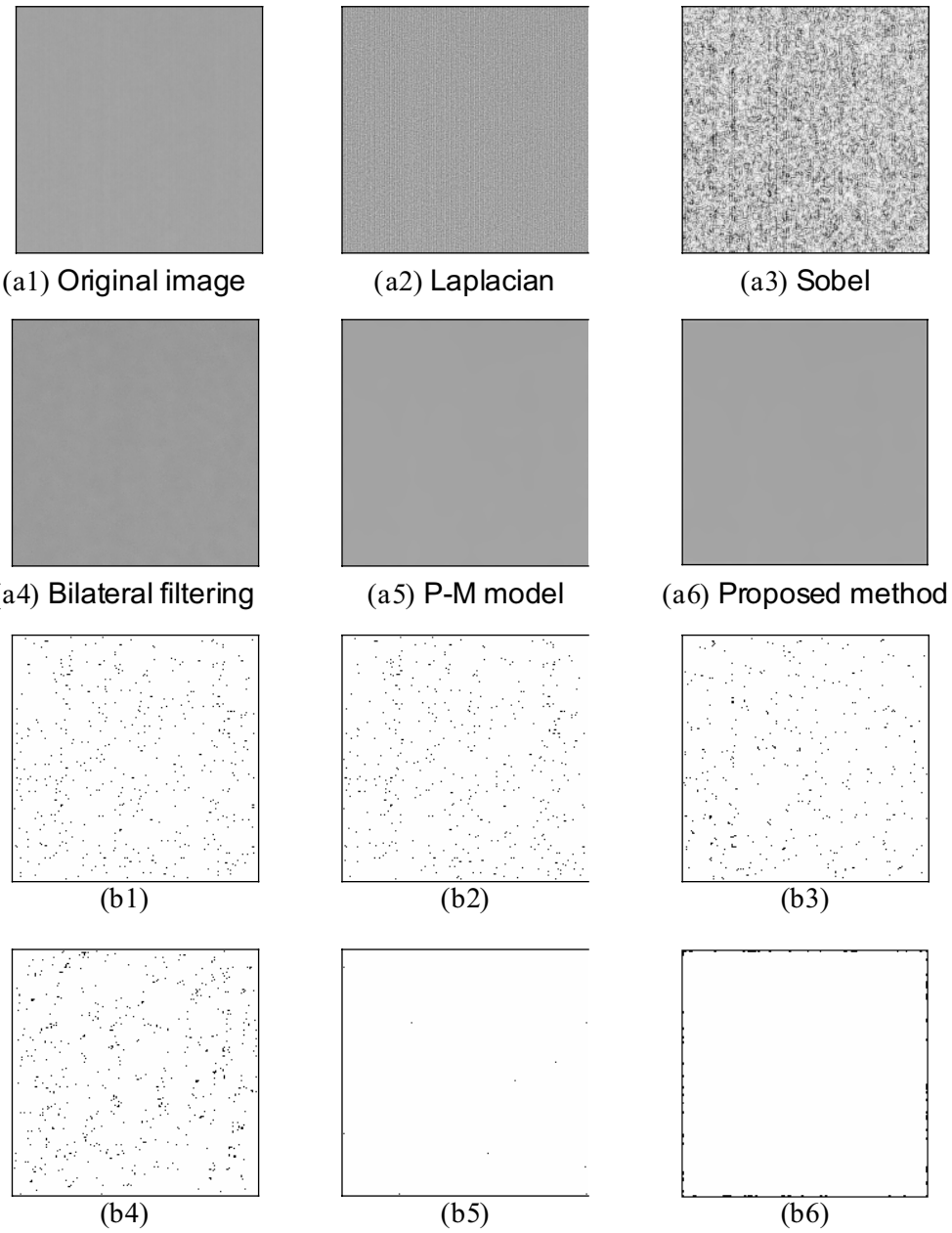

Figure 12. Comparison of various filtering methods for a faultless backlight panel sample: (a1) original image; (a2) result from Laplacian sharpening filter; (a3) result from Sobel edge detection; (a4) result from bilateral filtering; (a5) result from the P-M diffusion model; (a6) result from the proposed diffusion method; (b1)-(b6) thresholding results using 3-sigma control limits for the images in (a1)-(a6), respectively.

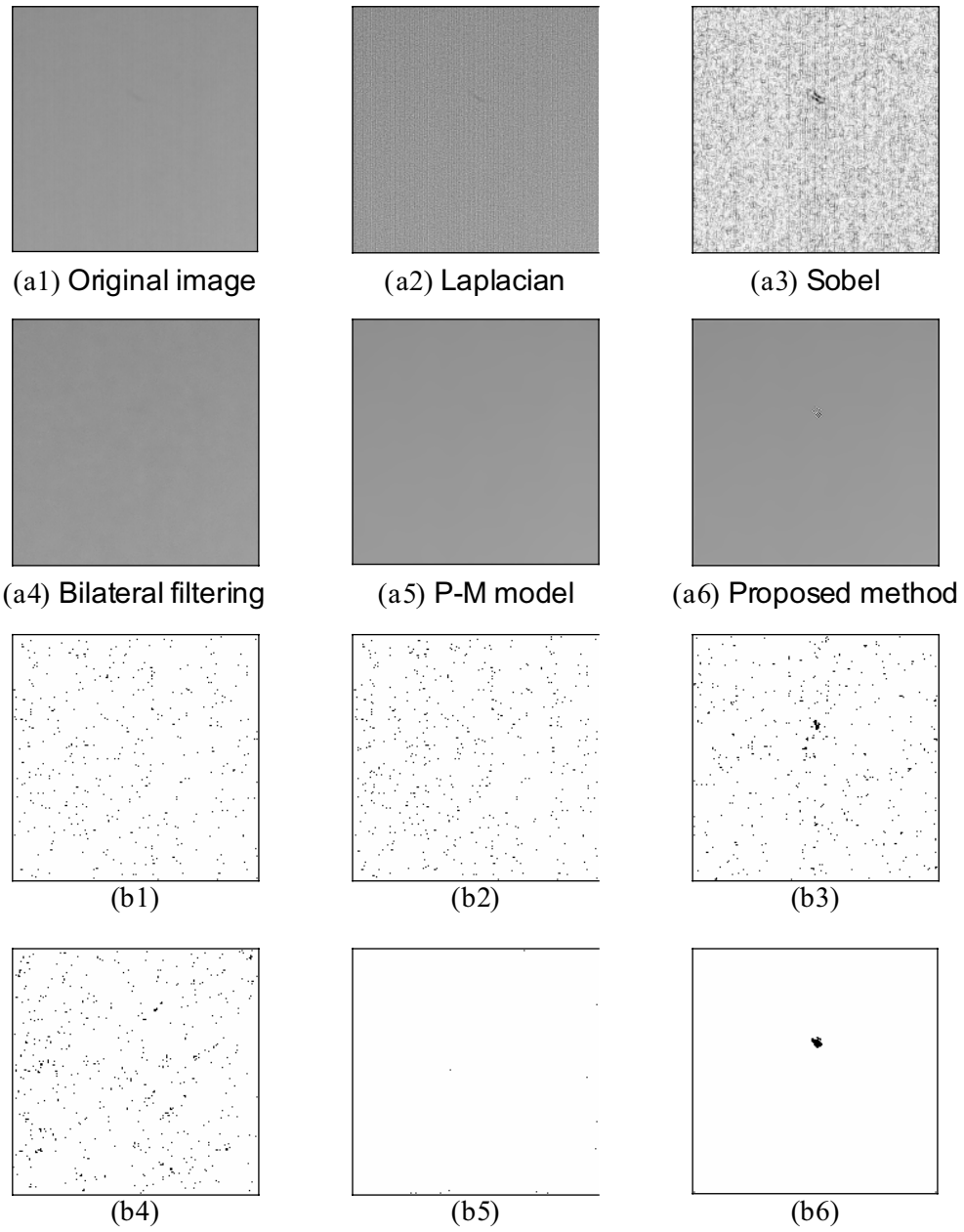

Figure 13. Comparison of various filtering methods for a defective backlight panel sample: (a1) original image; (a2) result from Laplacian sharpening filter; (a3) result from Sobel edge detection; (a4) result from bilateral filtering; (a5) result from the P-M diffusion model; (a6) result from the proposed diffusion method; (b1)-(b6) thresholding results using 3-sigma control limits for the images in (a1)-(a6), respectively.

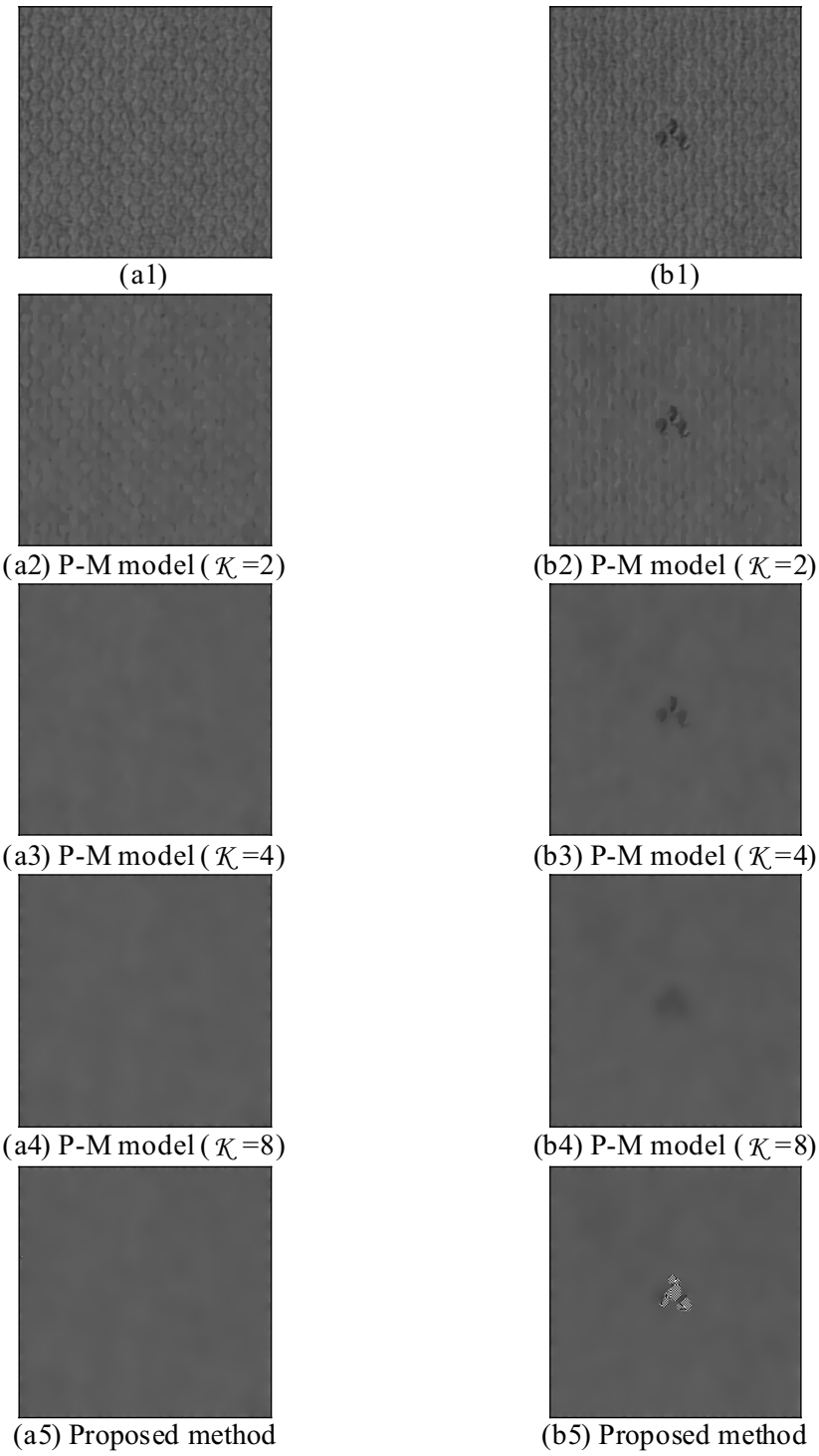

Figure 14. Diffusion results of texture images: (a1)-(b1) faultless and defective textile fabric images, respectively; (a2)-(a4) and (b2)-(b4) detection results from the P-M diffusion model with $\mathcal{K}$ = 2, 4 and 8 for (a1) and (b1), respectively; (a5), (b5) detection results from the proposed diffusion model with α = 0.2 and $\mathcal{K}$ = 8. (Number of iterations = 30 for all test samples.)